Supplement of Biogeosciences, 17, 2701–2714, 2020
https://doi.org/10.5194/bg-17-2701-2020-supplement

Biogeosciences
Open Access

Supplement of

Quantifying the contributions of riverine vs. oceanic nitrogen to hypoxia in the East China Sea

Fabian Große et al.

Correspondence to: Fabian Große (fabian.grosse@dal.ca)

S1 River input locations

Table S1. Center coordinates of input grid cells of all rivers considered in this study and their associated nitrogen source groups. 'None' in last column indicates nitrogen from the river was not explicitly labeled as the river is outside of the tracing region (see Fig. 1, main text).

River name	Latitude (°N)	Longitude (°E)	Source group
Liaohe	40.83	121.75	None
Yalujiang	39.75	124.25	None
Luanhe	39.42	119.33	None
Haihe	39.00	117.83	None
Yellow River	37.58	119.08	None
Hanjiang	37.42	126.42	None
Huaihe	34.00	120.42	None
Changjiang	31.67	121.08	Changjiang
Qiantangjiang	30.25	120.92	Other rivers
Oujiang	27.83	120.92	Other rivers
Minjiang	26.00	119.75	Other rivers

S2 Simulated circulation in the East China Sea

Zhang et al. (in review, 2019) assessed the skill of the applied ROMS model with respect to the physics based on sea surface temperature and salinity, which provides a basic validation of the simulated hydrography. However, our study of the contributions of the different nutrient sources on hypoxia also requires a good representation of the general circulation in the East China Sea (ECS). This is particularly important considering the distinct seasonality of the region due to the East Asian monsoon. Furthermore, it is important to evaluate simulated surface and subsurface currents as intrusion from the Kuroshio occur mainly in the subsurface (Zhou et al., 2017a, 2018). Therefore, Fig. S1 shows average ocean current velocities and directions in the surface (0–25 m; panels a, b) and subsurface ocean (25–200 m; panels c, d) during summer (June to August, 'JJA'; panels a, c) and winter (December to February, 'DJF'; panels b, d) 2008–2013. The main branch of the Kuroshio is well reproduced, visible as a band of high current velocities in the surface and subsurface (Figs. S1a, b). Maximum velocities of up to $1.6\,\mathrm{m\,s^{-1}}$ occur during summer in the surface layers directly east of Taiwan (Fig. S1a). North of Taiwan, summer currents are driven mainly by inflow through Taiwan Strait, indicated by the band of relatively high velocities off the Chinese coast (Figs. S1a, b). At about 27.5 °N, 122.5 °E, the current merges with a subsurface intrusion from the Kuroshio branching northeast of Taiwan (Fig. S1b). This current is partly deflected northeastward at 29 °N, which is in agreement with both another model (Bian et al., 2013) and observations (Zhou et al., 2017b, 2018).

North of 31 °N, the southward Yellow Sea Coastal Current (YSCC) is simulated in summer and winter (Figs. S1a and b, respectively), but it is weaker and reaches less far south in summer. This behavior is within the range of existing modeling studies, which either simulate a consistent northward current (Bian et al., 2013) or a seasonal reversal of the YSCC (Guo et al., 2006). Existing observations are inconclusive on the seasonality of the YSCC (Bian et al., 2013).

The surface inflow through Taiwan Strait is significantly lower in winter than in summer (compare Figs. S1a and c), due to the southwestward flowing East China Sea Coastal Current with velocities of 0.1–$0.3\,\mathrm{m\,s^{-1}}$, which is in line with Bian et al. (2013).

The subsurface Kuroshio intrusion northeast of Taiwan is also present in winter (Fig. S1d), but reaches less far north than during summer. A relatively strong westward current (up to $0.4\,\mathrm{m\,s^{-1}}$) at 125 °E, 31–32 °N originating from the Kuroshio is simulated in winter in both the surface and the subsurface (Figs. S1c, d). This is in agreement with model results of Guo et al. (2006), despite slightly higher current velocities in our model.

In summary, our model agrees well with existing literature with respect to the seasonality of surface and subsurface currents in the ECS. Thus, it provides a reliable basis for the source-specific nitrogen tracing.

S3 Spatial patterns of dissolved inorganic nitrogen

A good representation of the spatial gradients and temporal variability of nitrogen (N) concentrations in the ECS is important for reliable results of the N tracing applied in this study. Therefore, Figures S2 and S3 show spatial distributions of simulated and observed concentrations of dissolved inorganic nitrogen (DIN; nitrate + nitrite + ammonium) in the surface and bottom layers of the East China Sea off the Changjiang estuary. The observational data were collected during nine individual cruises in 2010, 2011 and 2012 (for details see Gao et al. (2015)). The simulated DIN concentrations are averaged over the individual survey periods.

The model reproduces the general spatial patterns of DIN both at the surface (Fig. S2) and at the bottom (Fig. S3), especially with respect to the strong horizontal gradient between the Changjiang plume and the oceanic offshore waters. The same applies to the temporal variability across the different cruises. The good model-data agreement is further illustrated by the strong correlation between simulated and observed DIN concentrations at both surface and bottom (see Fig. S4).

S4 Source-specific gross oxygen consumption in northern and southern region

Table S2 provides the values for gross oxygen consumption (GOC), its relative contributions by the different N sources and total hypoxic areas for the northern and southern regions

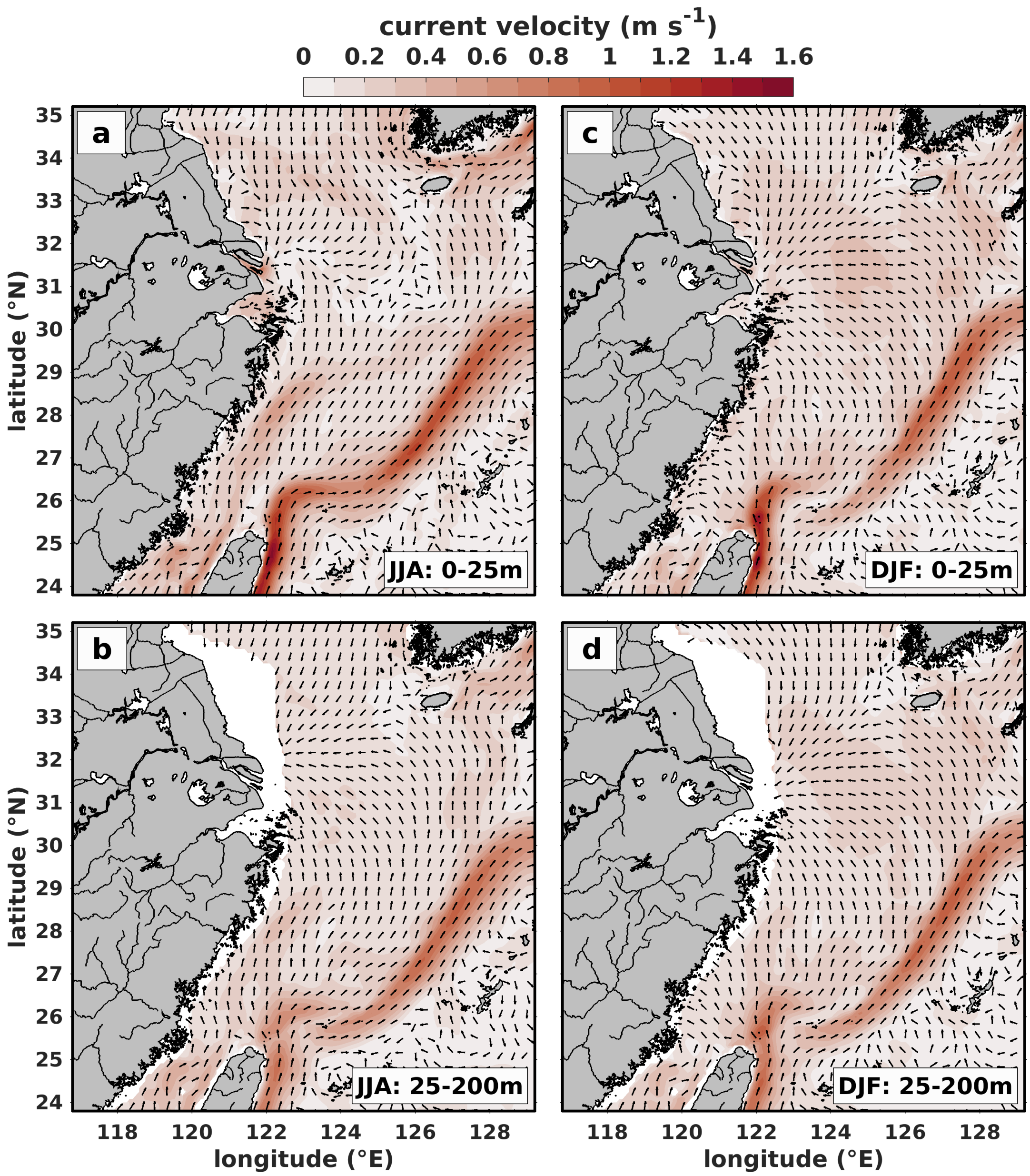

Figure S1. Temporally (2008–2013) and vertically averaged ocean current directions (arrows) and velocities (colors) near the surface (0–25m; a, c) and in the subsurface ocean (25–200m; b, d) during summer (June–August (JJA); a, b) and winter (December–February (DJF); c, d). Direction vectors are sampled every four grid cells and have the same length. Same color scale for all panels.

corresponding to the analyses presented in section 3.3 of the main text. Table S3 provides the analogous values and wind velocities corresponding to the results presented in section 3.4 of the main text.

S5 Seasonal cycle of freshwater thickness and stratification

To study the effect of the Changjiang freshwater (FW) on stratification, we calculate the FW thickness using the passive dye tracers from the Changjiang. The FW thickness at a specific location (x,y,t) is defined as (Zhang et al., 2012):

$$h_{fw} = \int_{-z_0}^{\eta} C_p \, dz \qquad \text{(S1)}$$

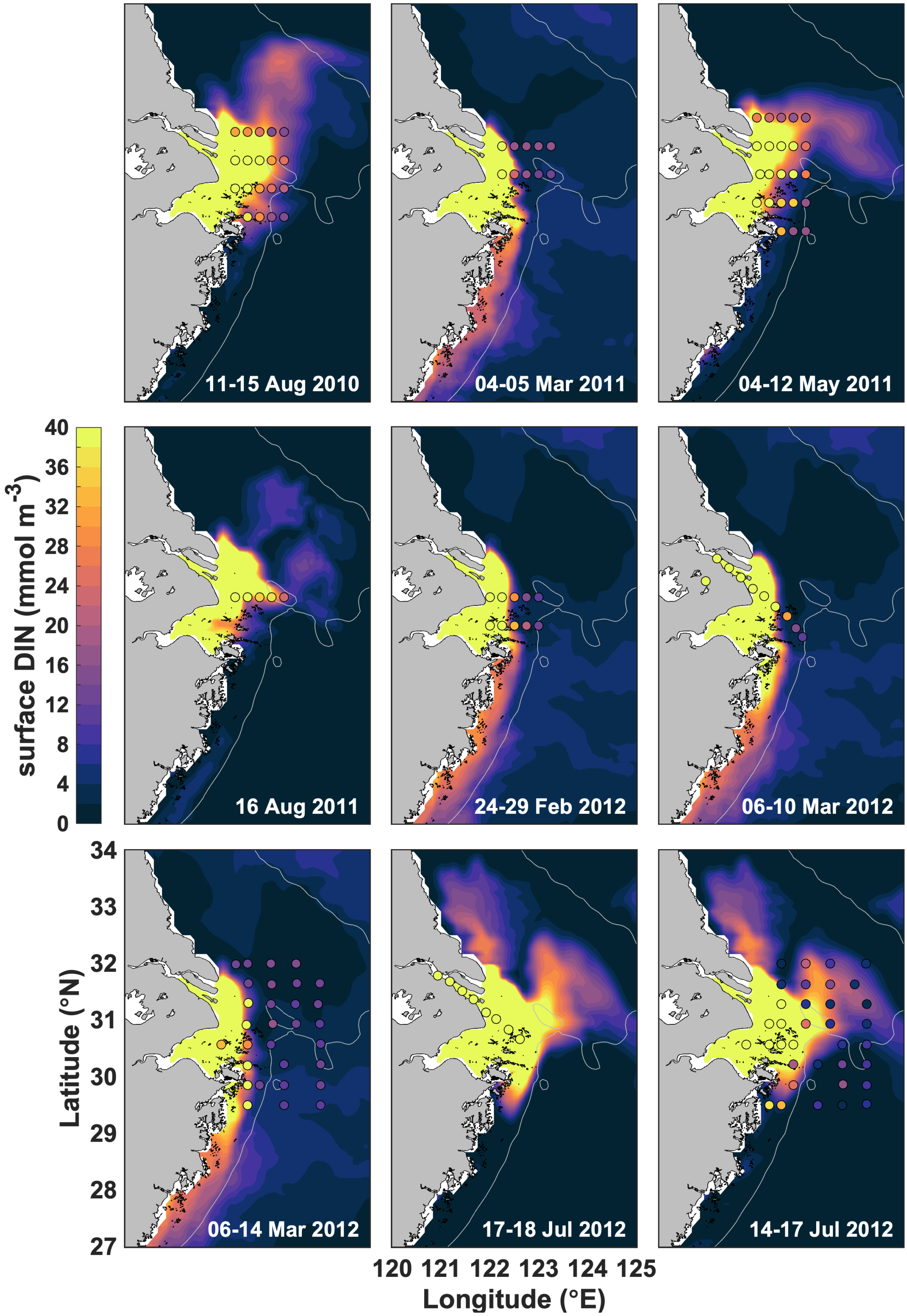

Figure S2. Spatial distributions of simulated (contours) and observed concentrations (circles) of dissolved inorganic nitrogen (DIN; nitrate + nitrite + ammonium) in the surface layer during nine cruises off the Changjiang estuary. Simulated values are averaged over the survey periods given in each panel and are taken from the model's surface grid cells. Sample data are taken from Gao et al. (2015). Same color scale for all panels.

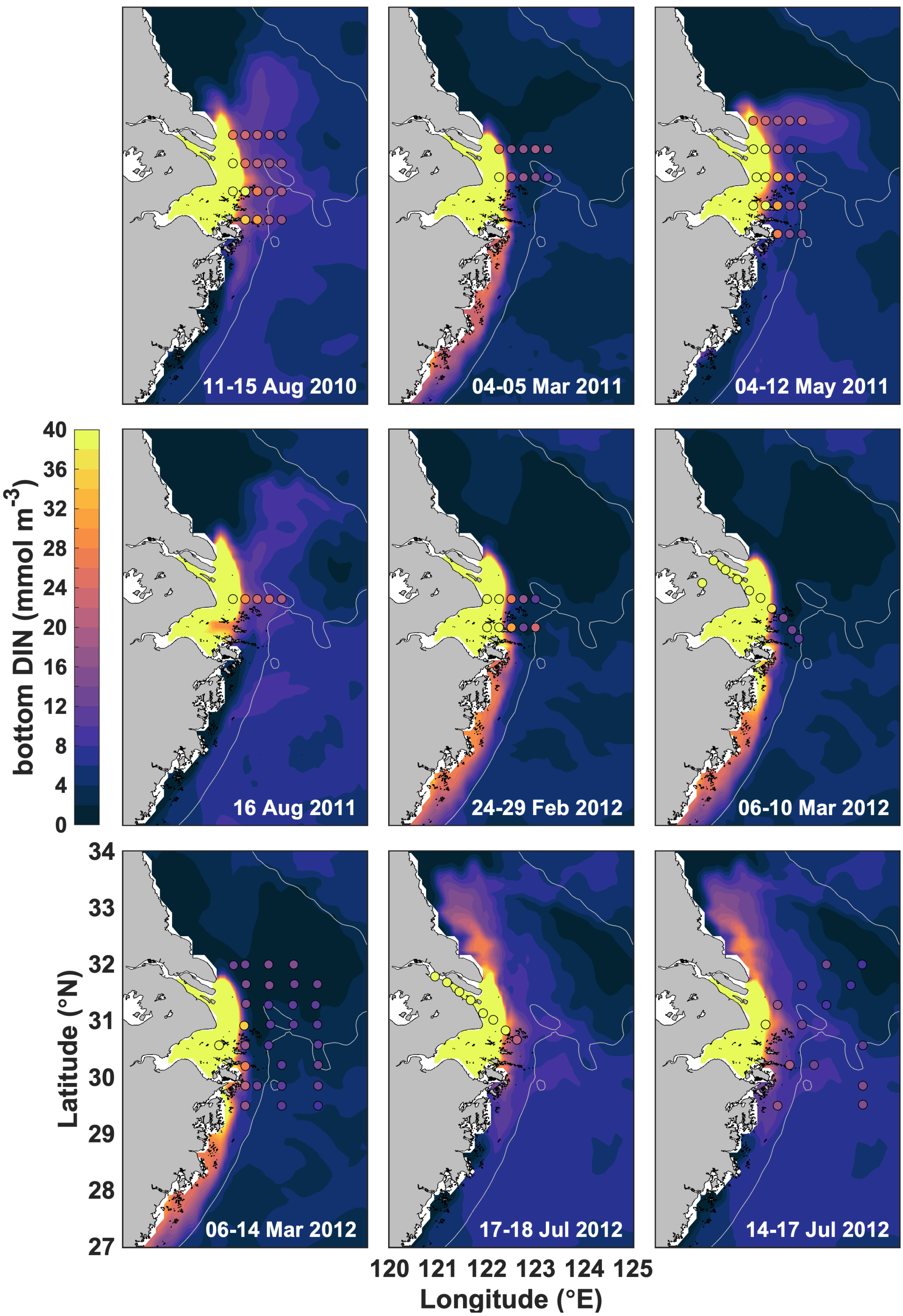

Figure S3. Same as Fig. S2 but for the bottom layer.

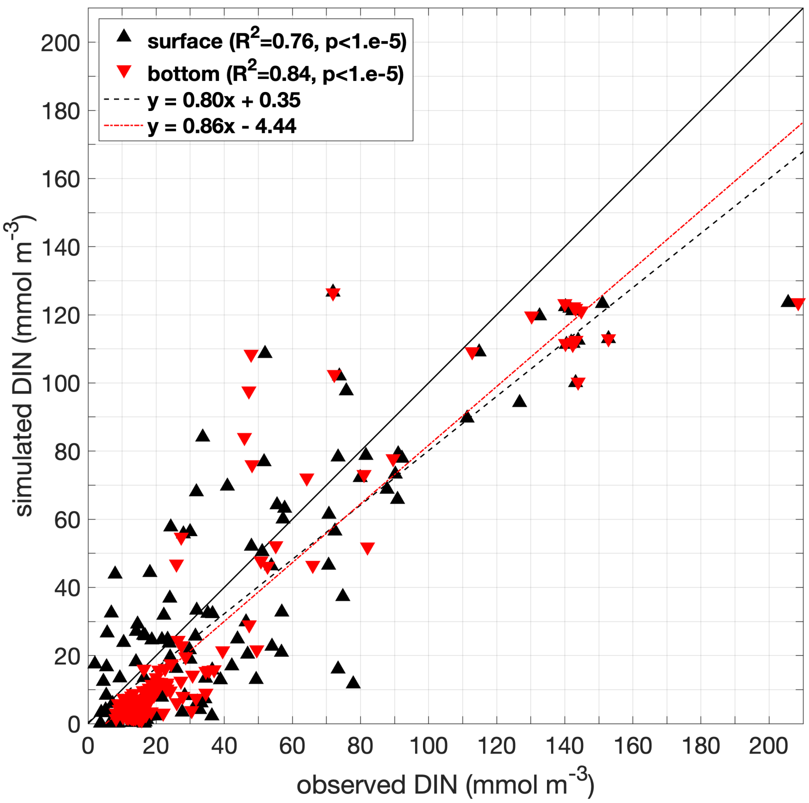

Figure S4. Scatter plot of simulated over observed dissolved inorganic nitrogen (DIN) concentrations corresponding to Figs. S2 and S3. Solid line represents one-to-one agreement. Dashed and dash-dotted lines represent linear fits for surface and bottom DIN, respectively.

Table S2. Average gross oxygen consumption (GOC; in $\mathrm{mmol\,O_2\,m^{-2}\,d^{-1}}$), its source-specific contributions (in %) and total hypoxic area (A_H; in $10^3\,\mathrm{km}^2$) in the northern and southern analysis regions (see Fig. 1, main text) during July to November of the years 2008–2013 and averaged (± 1 standard deviation) over the entire period. Values for GOC and A_H correspond to Fig. 4 in the main text. Yellow Sea contribution is not shown (always <0.2%). Percentage sums greater than 100% due to rounding.

Year	GOC	Changjiang	Other rivers	Kuroshio	Taiwan Strait	A_H
			northern region			
2008	51.6	75.0	4.2	14.8	5.9	8.0
2009	52.4	78.1	3.7	12.7	5.6	8.4
2010	52.5	78.2	4.0	12.1	5.6	14.4
2011	50.9	71.2	4.6	17.2	6.9	8.4
2012	54.2	77.5	4.2	12.4	5.9	8.5
2013	51.5	63.3	3.6	22.4	10.7	0.5
mean	52.2 ± 1.2	73.9 ± 5.4	4.0 ± 0.3	15.2 ± 3.7	6.8 ± 1.8	8.0 ± 4.4
			southern region			
2008	42.3	60.3	4.4	19.0	16.3	12.3
2009	41.9	61.1	4.7	17.8	16.5	10.5
2010	40.0	58.4	4.9	17.9	18.7	12.0
2011	38.6	51.9	4.6	22.3	21.2	5.7
2012	41.8	60.2	5.1	17.7	17.1	6.3
2013	32.4	46.9	4.2	23.2	25.6	4.6
mean	39.5 ± 3.8	56.9 ± 5.1	4.7 ± 0.3	19.5 ± 2.2	18.9 ± 3.2	8.6 ± 3.4

Table S3. Monthly averaged gross oxygen consumption (GOC; in $\mathrm{mmol\,O_2\,m^{-2}\,d^{-1}}$), relative contributions by different N sources (in %), hypoxic area (A_H; in $10^3\,\mathrm{km}^2$), and meridional wind (v_{10}; in $\mathrm{m\,s^{-1}}$) in the southern region in 2008 and 2013. Values correspond to results shown in Fig. 5 (main text). Yellow Sea contribution not shown (always <0.2%). Percentage sums greater than 100% due to rounding.

Month	GOC	Changjiang	Other rivers	Kuroshio	Taiwan Strait	A_H	v_{10}
				2008			
1	15.0	67.9	3.4	14.1	14.5	0.0	-6.5
2	6.0	66.5	3.4	16.0	14.0	0.0	-6.6
3	30.5	66.1	4.5	13.1	16.1	0.0	-2.6
4	33.7	66.3	5.8	12.6	15.1	0.0	-1.0
5	20.0	42.1	7.2	22.3	28.4	0.1	-0.3
6	23.2	34.2	11.2	27.9	26.7	0.1	3.0
7	35.1	28.7	7.5	33.1	30.8	1.0	4.6
8	43.9	37.0	6.3	31.2	25.4	1.5	1.9
9	67.0	76.2	3.4	11.6	8.8	8.0	-1.5
10	42.1	77.4	2.3	11.1	9.3	7.9	-3.3
11	23.7	76.7	2.5	9.5	11.3	6.7	-5.4
12	23.9	74.7	2.5	9.8	13.0	0.0	-4.7
mean	30.4 ± 15.8	60.0 ± 19.4	4.9 ± 2.5	17.8 ± 9.2	17.2 ± 8.3	2.1 ± 3.3	-1.8±3.7
				2013			
1	6.6	75.3	2.8	11.8	10.1	0.0	-4.8
2	12.4	74.8	3.4	11.6	10.2	0.0	-4.0
3	29.1	67.4	4.1	14.3	14.2	0.0	-2.5
4	38.5	67.5	5.2	13.8	13.5	0.0	-1.1
5	22.8	55.6	7.1	17.9	19.4	0.0	0.9
6	39.6	62.9	8.8	14.1	14.2	1.6	1.2
7	27.6	35.8	6.6	21.2	36.3	4.3	5.9
8	26.7	2.2	2.6	42.9	52.3	0.1	3.4
9	49.1	56.8	5.3	20.5	17.4	0.5	-3.3
10	34.2	61.9	3.1	19.4	15.6	0.4	-6.6
11	24.6	68.8	2.9	14.4	13.9	0.0	-4.2
12	20.6	72.7	3.6	9.6	14.1	0.0	-6.1
mean	27.7 ± 11.7	56.8 ± 19.7	5.0 ± 2.0	18.4 ± 8.4	19.9 ± 12.1	0.6 ± 1.3	-1.7 ± 3.9

Here, η and z_0 are the sea surface elevation at (x,y,t) and the reference depth down to which the dye tracer concentration C_p attributed to Changjiang is integrated, respectively. We use $z_0 = 25\,\mathrm{m}$ as the amount of FW in the near-surface layers is the most relevant for stratification.

We use potential energy anomaly (PEA; Simpson, 1981), a measure for the stability of a water column, to analyze stratification:

$$\mathrm{PEA} = \frac{1}{D} \int_{-H}^{\eta} gz\left(\overline{\rho} - \rho\right)\,dz, \tag{S2}$$

with water column depth $D = -H + \eta$, bottom depth H, local depth z, gravitational acceleration g, potential density ρ, and vertically averaged potential density $\overline{\rho}$:

$$\overline{\rho} = \frac{1}{D} \int_{-H}^{\eta} \rho\,dz. \tag{S3}$$

Density ρ depends on salinity (S), temperature (T) and pressure (p), and is calculated from the simulated fields using the'Thermodynamic Equation of Seawater' (TEOS-10; McDougall and Barker, 2011):

$$\rho = \rho\,(S,T,p)\,. \tag{S4}$$

To analyze the effect of Changjiang FW on stratification in the highly variable southern hypoxic region (see main text, Fig. 1), we present time series of monthly and spatially averaged FW thicknesses and PEA over water depth (PEA/D) for that region for the years of the largest (2008) and smallest simulated hypoxic areas (2013) in Fig. S5. We use PEA/D instead of PEA as PEA increases with increasing water depth D, which would give stronger weight to deeper regions within the analysis regions.

The FW thickness shows a distinct seasonal cycle with low values during July/August, a strong increase in September/October, followed by a decrease through winter and spring. Only in 2013, this pattern is interrupted by a short-term increase of FW thickness in June. The seasonal cycle of

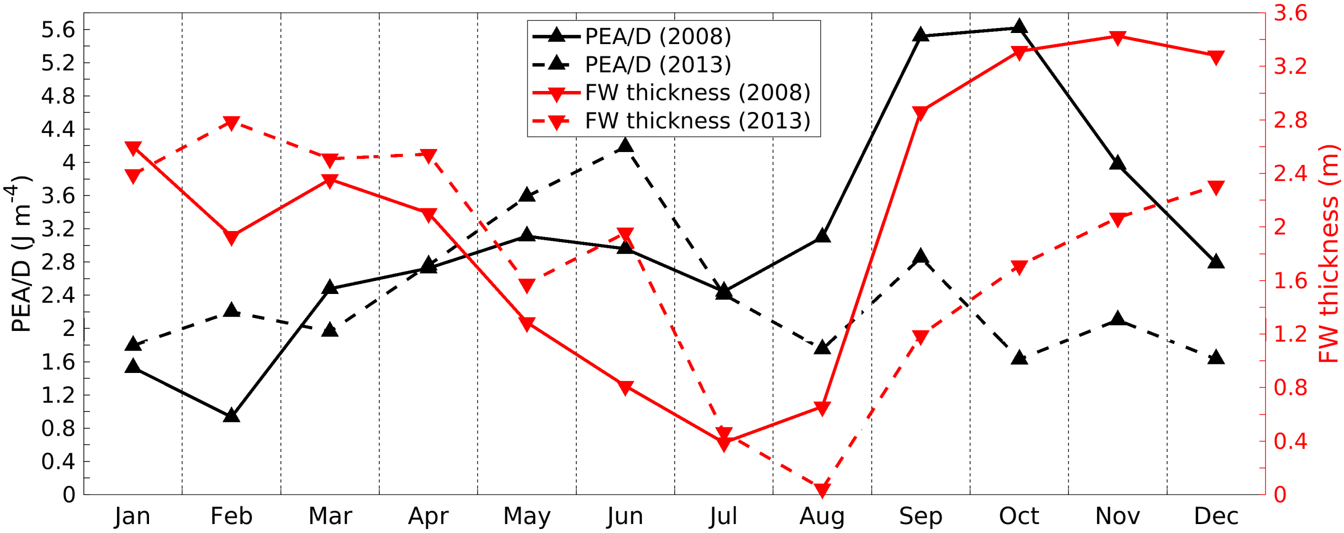

Figure S5. Monthly averaged freshwater (FW) thickness (in upper 25 m) and potential energy anomaly over water depth (PEA/D) in the southern region for the years of the largest (2008) and smallest (2013) hypoxic areas.

PEA/D is less pronounced, and partly opposed to that of FW thickness. PEA/D tends to increase from January to June, although FW thickness steadily decreases, which likely results from surface warming and an inflow of oceanic water masses in the subsurface (see Fig. S1b) supporting an increase in stratification.

The strong increase in FW thickness during September of both years coincides with an increase in PEA/D, which is particularly pronounced in 2008, the year of the largest hypoxic area. This is caused by both the higher Changjiang FW discharge compared to 2013 (see main text, Fig. 2) and the anomalously weak winds in September/October 2008 (see Fig. 5), which enable the longer maintenance of intense stratification. In contrast, the winds are anomalously strong in September 2013, and FW thickness is almost 2 m less than in 2008 (see Fig. S5b), resulting in only a minor increase in stratification.

S6 Simulated surface currents during June and October of 2008 and 2013

To illustrate the effect of year-to-year variations in the synoptic wind patterns on water mass transport, Fig. S6 presents monthly averaged simulated surface currents (0–25 m) during June and October of 2008 and 2013. The northward wind component in June 2008 was anomalously strong, while in June 2008 it was particularly weak (see Fig. 5, main text). This is reflected in the surface currents during both years. In June 2008 (Fig. S6a), the surface currents are consistently northward in the regions south of 31 °N. In contrast, the northward component of the coastal current is much weaker in June 2013, and even turns into a southward current directly onshore. This enables the southward transport of Changjiang FW in June 2013 and supports the short-term increase in stratification and GOC in the southern hypoxia region (see Figs. S5 and 5, respectively).

Similarly, the anomalously weak southward winds in October 2008 result in a weaker southward coastal current (Fig. S6b) compared to October 2013, when the southward winds are particularly strong (see Fig. 5, main text). These variations in the surface currents in response to variability in the meridional winds explain the differences in FW thickness and GOC supported by N from the Changjiang between October 2008 and 2013 shown in Figs. S5 and 5, respectively.

S7 Seasonal cycle of oxygen consumption and hypoxia in the southern region under 50% reduced Changjiang N loads

Figure S7 presents monthly time series of source-specific GOC and total hypoxic area in the southern analysis region (see main text, Fig. 1) for 2008 and 2013. In addition, it shows the 6-year monthly average of the meridional wind speed 10 m above sea level (v_{10}) and the corresponding anomalies for both years (analogous to main text, Fig. 5).

References

Bian, C., Jiang, W., and Greatbatch, R. J.: An exploratory model study of sediment transport sources and deposits in the Bohai Sea, Yellow Sea, and East China Sea, J. Geophys. Res.-Oceans, 118, 5908–5923, https://doi.org/10.1002/2013JC009116, 2013.

Gao, L., Li, D., Ishizaka, J., Zhang, Y., Zong, H., and Guo, L.: Nutrient dynamics across the river-sea interface in the Changjiang

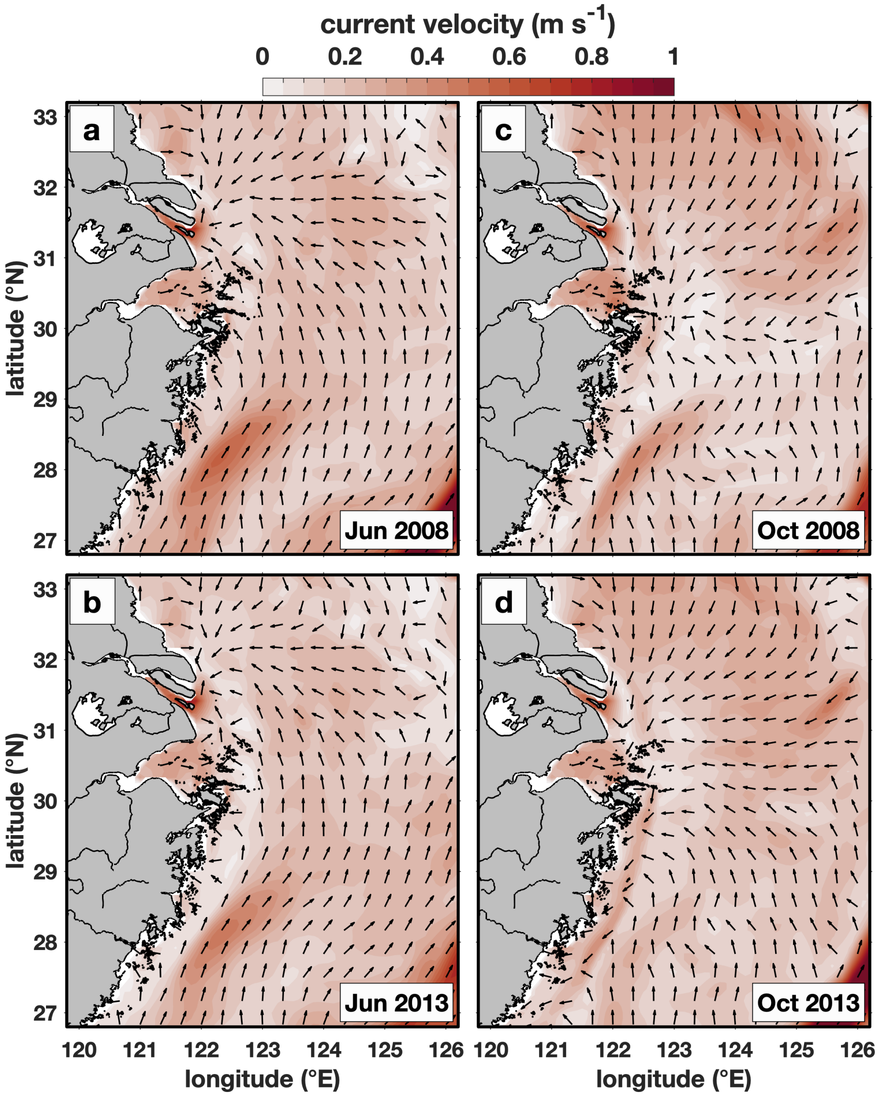

Figure S6. Monthly and vertically (0–25 m) averaged ocean current directions (arrows) and velocities (colors) in June (a, b) and October (c, d) of 2008 (a, c) and 2013 (b, d). Direction vectors are sampled every four grid cells and have the same length.

(Yangtze River) estuary—East China Sea region, Limnol. Oceanogr., 60, 2207–2221, https://doi.org/10.1002/lno.10196, 2015.

Guo, X., Miyazawa, Y., and Yamagata, T.: The Kuroshio onshore intrusion along the shelf break of the East China Sea: The origin of the Tsushima Warm Current, J. Phys. Oceanogr., 36, 2205–2231, https://doi.org/10.1175/JPO2976.1, 2006.

McDougall, T. J. and Barker, P. M.: Getting started with TEOS-10 and the Gibbs Seawater (GSW) oceanographic toolbox, Tech. rep., SCOR/IAPSO, http://www.teos-10.org/pubs/gsw/v3_04/pdf/Getting_Started.pdf, 2011.

Simpson, J. H.: The shelf-sea fronts: implications of their existence and behaviour, Philos. T. Roy. Soc. A, 302, 531–546, https://doi.org/10.1098/rsta.1981.0181, 1981.

Zhang, H., Fennel, K., Laurent, A., and Bian, C.: A numerical model study of the main factors contributing to hypoxia and its sub-seasonal to interannual variability off the Changjiang Estuary, Biogeosciences Discuss., https://doi.org/10.5194/bg-2019-341, in review, 2019.

Zhang, X., Hetland, R. D., Marta-Almeida, M., and DiMarco, S. F.: A numerical investigation of the Mississippi and Atchafalaya freshwater transport, filling and flushing times on the Texas-Louisiana Shelf, J. Geophys. Res.-Oceans, 117, C11 009, https://doi.org/10.1029/2012JC008108, 2012.

Zhou, F., Chai, F., Huang, D., Xue, H., Chen, J., Xiu, P., Xuan, J., Li, J., Zeng, D., Ni, X., and Wang, K.: Investigation of hypoxia off the Changjiang Estuary using a coupled model of ROMS-CoSiNE, Prog. Oceanogr., 159, 237–254, https://doi.org/10.1016/j.pocean.2017.10.008, 2017a.

Zhou, P., Song, X., Yuan, Y., Wang, W., Cao, X., and Yu, Z.: Intrusion pattern of the Kuroshio Subsurface Water onto the East China Sea continental shelf traced by dissolved inorganic iodine

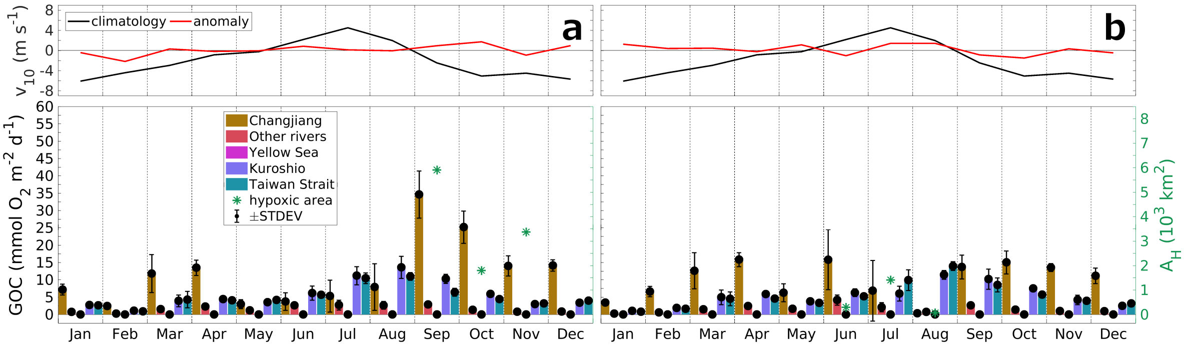

Figure S7. Monthly time series of source-specific contributions to GOC and total hypoxic area (A_H) in the southern region (see main text, Fig. 1) under 50% reduced Changjiang N loads in (a) 2008 (year of largest A_H) and (b) 2013 (smallest A_H), and anomaly of northward wind speed 10 m above sea level (v_{10}) relative to 2008–2013 (‘climatology’) averaged over the ECS (25–33 °N, 119–125 °E). Same legend and axes for both panels.

species during the spring and autumn of 2014, Mar. Chem., 196, 24–34, https://doi.org/10.1016/j.marchem.2017.07.006, 2017b.

Zhou, P., Song, X., Yuan, Y., Wang, W., Chi, L., Cao, X., and Yu, Z.: Intrusion of the Kuroshio Subsurface Water in the southern East China Sea and its variation in 2014 and 2015 traced by dissolved inorganic iodine species, Prog. Oceanogr., 165, 287–298, https://doi.org/10.1016/j.pocean.2018.06.011, 2018.